

Rapid identification of sand-size mineral grains using portable XRF: A new method for indicator mineral surveys



Alexei S. Rukhlov^{1, a}, Mao Mao¹, and Christina Rippon²

¹ British Columbia Geological Survey, Ministry of Energy, Mines and Petroleum Resources, Victoria, BC, V8W 9N3

² School of Earth and Ocean Sciences, University of Victoria, Victoria, BC, V8P 5C2

^a corresponding author: Alexei.Rukhlov@gov.bc.ca

Recommended citation: Rukhlov, A.S., Mao, M., and Rippon, C., 2018. Rapid identification of sand-size mineral grains using portable XRF: A new method for indicator mineral surveys. In: Geological Fieldwork 2017, British Columbia Ministry of Energy, Mines and Petroleum Resources, British Columbia Geological Survey Paper 2018-1, pp. 167-182.

Abstract

Qualitative portable X-ray fluorescence (pXRF) offers a novel method of rapid, non-destructive identification of sand-size, single mineral grains. Using a (pXRF) instrument on 60 single-grain (0.5-1.0 mm) samples comprising 17 different rock-forming and accessory minerals, we detected essential constituents that readily identify ambiguous grains recovered from concentrates (e.g., Ca-P for apatite, Ca-Ti-Si for titanite, Ca-Nb-Ta for pyrochlore). Thus real-time readings (30-150 s) from a factory-calibrated instrument can help identify separated sand-sized single mineral grains in the field or laboratory. Considering the popularity of pXRF instruments, this simple method will be useful in mineral exploration and in other areas using mineral separates, such as industrial mineral, geochronologic, and provenance studies.

Keywords: Portable energy dispersive X-ray fluorescence (ED-XRF) spectrometry, pXRF, non-destructive analysis, X-ray emission spectra, indicator minerals, REE, Nb, Ta, Zr, Ti, apatite, olivine, zircon, titanite, ilmenite, pyrochlore, ferrocolumbite, zirconolite, alkali feldspar, amphibole, pyroxene, nepheline

1. Introduction

Geochemical surveys using dispersal of heavy (>2.8 g-cm⁻³) and indicator minerals in drainage and glacial sediments are long-established methods of mineral exploration in regions covered by extensive overburden (e.g., Averill, 2001; McClenaghan, 2005; Gent et al., 2011; Lett and Rukhlov, 2017). Generally resistant to abrasion during glacial transport and weathering, indicator minerals characteristic of a specific ore deposit or alteration type can be detected across a greater area than the source. Mineral fractions are recovered from rocks and sediments for prospecting and for geochronologic, detrital provenance, mineral chemistry, and tracer isotopic studies. Indicator minerals are typically identified and counted by hand-picking under a binocular microscope. Fractions (typically 0.25-0.50, 0.5-1.0, and 1-2 mm) are recovered by on-site screening and panning and by laboratory processing of bulk samples using shaking tables, magnetic separators, and heavy liquids (e.g., McClenaghan et al., 2014; Plouffe et al., 2014). Although modern automated techniques such as MLA (Mineral Liberation Analysis) and QEMSCAN[®] (Quantitative Evaluation of Materials by SCANNing electron microscopy; see Layton-Matthews et al., 2014 for an overview) allow rapid modal analysis of even finer-grained fractions (e.g., Mackay et al., 2016), many applications still use hand-picked mineral fractions.

Visually identifying small mineral grains can be a challenge, especially for worn detrital grains. Quantitative sorting of mineral grains thus requires more sophisticated methods,

either optical, using immersion liquids, or analytical, using for example, X-ray diffraction, scanning electron microscopy with energy-dispersive X-ray spectrometry (SEM-EDS) or reflectance spectroscopy. However, some of these methods destroy the sample, need additional sample preparation (e.g., grain mounts), and require costly laboratory equipment and time-consuming procedures. Having a rapid, in-field technique to confirm ambiguous mineral grains would be beneficial to prospecting and regional indicator mineral surveys.

Energy dispersive X-ray fluorescence (ED-XRF) spectrometry is a well-established method of rapid, non-destructive, multi-elemental analysis, whereby X-rays generated by an anode tube excite electrons in sample atoms, resulting in the emission of X-rays characteristic of specific elements (e.g., Piorek, 1994). Recent advances in the ED-XRF technology have made it field portable, and thus it has become an increasingly versatile technique for in situ geological, environmental, pedological, archaeological and other applications (e.g., Bishop et al., 2004; Glanzman and Closs, 2007; Potts and West, 2008; Palmer et al., 2009; Liritzis and Zacharias, 2011; Chen et al., 2013; Weindorf et al., 2013; Wiedenbeck, 2013; Simandl et al., 2014; Quye-Sawyer et al., 2015; Sarala et al., 2015; Chiari et al., 2016; Martín-Peinado and Rodríguez-Tovar, 2016; Young et al., 2016; Bull et al., 2017; Cohen et al., 2017; Ryan et al., 2017; Steiner et al., 2017; Zhang et al., 2017). Modern portable X-ray fluorescence (pXRF) spectrometers are capable of achieving accuracy and precision of multi-elemental determinations comparable to those of larger XRF instruments and other

laboratory methods (e.g., Knight et al., 2013; Rukhlov, 2013; Rouillon and Taylor, 2016; Ryan et al., 2017; Steiner et al., 2017). Although pXRF has been widely used in mineral exploration for in-field and laboratory analysis of different types of media such as rocks, drill cuttings, sediments, and pulverized samples (e.g., Wiedenbeck, 2013; Simandl et al., 2014; Sarala et al., 2015), we are unaware of reported pXRF applications to sand-size, single mineral grains.

In this paper we propose a novel method of rapid, non-destructive identification of <1 mm-size, single mineral grains by qualitative pXRF. Relative proportions of essential elements readily identify minerals (e.g., Ca-P for apatite, Fe-Nb for ferrocolumbite). Real-time readings (30-150 s) from a factory-calibrated instrument help identify ambiguous grains in the field or laboratory. Considering the popularity of pXRF instruments, this simple method will be useful in mineral exploration and in other areas that require mineral fractions be rapidly identified, such as geochronologic, provenance, and mineral chemistry studies.

2. Materials and methods

Samples for this study comprised individual grains (mostly 0.5-1.0 mm) of known rock-forming and accessory minerals separated from carbonatites and associated silicate rocks of the Blue River area, east-central British Columbia (Pell, 1994; Table 1). Rock samples were examined in thin sections, and mineral compositions were subsequently confirmed by wavelength-dispersion, electron-probe micro-analysis (EPMA). Sample preparation and pXRF analyses were carried out in the British Columbia Geological Survey (BCGS) laboratory. Rock samples were crushed to <3 mm-size using a steel mill, sieved to 0.5-1.0 and 1-2 mm-size fractions, and the ferromagnetic fraction separated using an MRM-1 hand magnet. The 0.5-1.0 mm-size fraction was washed and processed in bromoform (CHBr_3 ; $\text{SG}=2.85 \text{ g}\cdot\text{cm}^{-3}$) into the light and heavy fractions, followed by hand-picking under a binocular microscope. In the field, panning would replace the heavy liquid processing step.

All measurements were carried out on a self-contained Thermo Scientific Niton FXL 950 ED-XRF instrument (Fig. 1) equipped with 50 kV, 200 μA , 4W silver X-ray anode and a proprietary GOLDD (Geometrically Optimized Large Area Drift Detector) high-resolution detection system, capable of low detection limit, high-precision measurement of up to 42 elements (from $Z=12$ to 92). The instrument software includes fully automated data correction and reduction protocols optimized for determining elemental concentrations ranging ppm to ~100 wt.% in soils and rocks (Thermo Scientific, 2011). Real-time concentration results are displayed for each analysis and stored, along with the raw X-ray counts, in the internal memory for offline interpretation.

At each start up (~2 min) the system self-calibrated the energy resolution of the detector. The instrument detector resolution averaged $155 \pm 3 \text{ eV}$ (1σ) over three-year period ($n=76$). Each sample was analyzed in a plastic cup (2.45 cm diameter) with a bottom made of ultra-thin ($4 \mu\text{m}$) polypropylene film held by

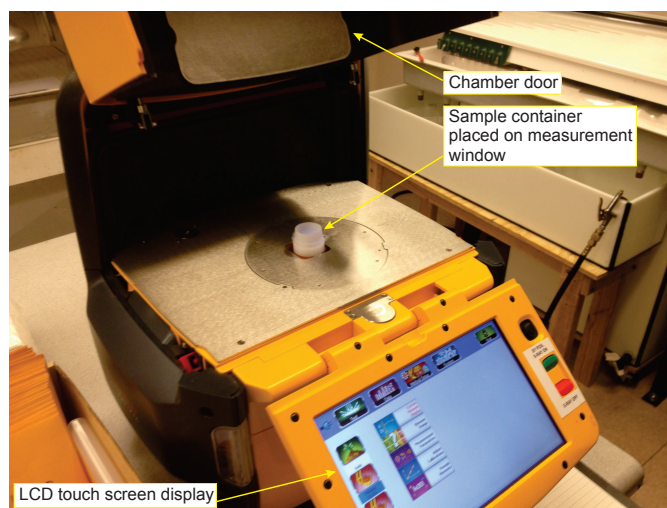


Fig. 1. Thermo Scientific Niton FXL 950 pXRF instrument and a sample container placed on the measurement window. A shielded sample chamber with an interlock system protects from X-ray radiation when the chamber door is closed and X-ray tube energized.

two concentric plastic rings (Fig. 2). The sample cup was placed onto the instrument measurement window so that mineral grain was centred above the 8 mm-diameter X-ray source (Fig. 1). For some measurements, air in the X-ray path was replaced with helium at a gas flow rate of $62.5 \text{ mL}\cdot\text{min}^{-1}$ to test if it would improve the detection of low atomic number elements such as Mg, Al, Si, P, S and Cl.

We used factory-calibrated ‘Mining Cu/Zn or Ta/Hf’ protocols based on fundamental parameters, because they measure a large number of elements with optimal sensitivity in different X-ray energy ranges via four excitation filters (Table 2; Thermo Scientific, 2011). Elements of the Main energy range were always measured, whereas the optional Low, High,

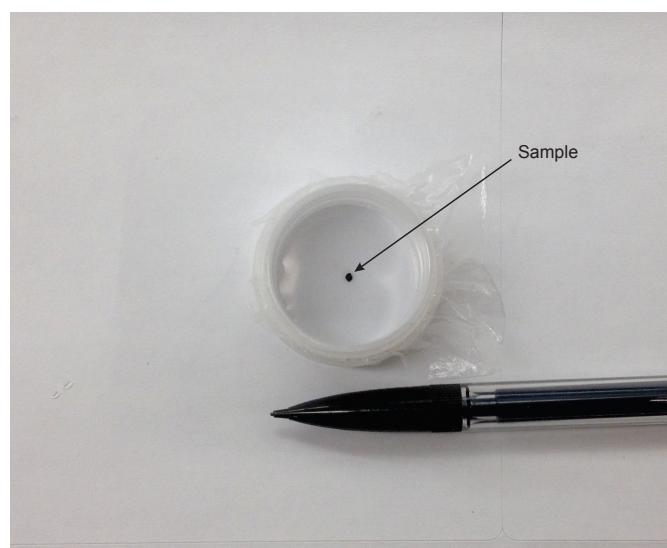


Fig. 2. Close-up of a sample holder (2.45 cm diameter) with a bottom made of ultra-thin ($4 \mu\text{m}$) polypropylene film held by two concentric plastic rings.

Table 1. Summary of minerals analyzed by pXRF as single grains. Essential elements detected are highlighted in bold.

Mineral	Source lithology	N ¹	Size fraction ²	General formula	Elements detected	Counting time ³
Albite	Fenites	5	0.5-1.0	(Na,Ca)[Al(Si,Al)Si ₂ O ₈]	Si, Ca ±Sr	105-150
Amphibole	Carbonatite	1	1.0	AB ₂ C ₅ [(Si,Al) ₈ O ₂₂](OH,F,Cl,O) ₂ A = Na, K; B = Li, Na, Mg, Fe, Mn, Ca; C = Li, Na, Mg, Fe, Mn, Al, Cr, Ti	Si, Fe, Ca, Mn	150
Apatite	Carbonatites, alkaline silicate rocks	13	0.5-1.0	A ₃ (BO ₄) ₃ (F,Cl,OH) A = Ca, Sr, Mn, Na, Y, REE ⁴ , Pb, Th, U; B = P, Si, S, As	P, Ca, Sr, Y ±S ±Ce ±Th	30-120
Calcite	Fenite	1	1.0	(Ca,Sr,Mg,Fe,Mn)CO ₃	Ca, Fe, Mn, Sr, Y	115
Dolomite	Carbonatites	2	0.5-1.0	(Ca,Sr)(Mg,Fe,Mn)(CO ₃) ₂	Ca, Fe, Mg, Mn, Sr	100
Fe sulphide	Carbonatite	1	1.0	Fe _{1-x} S – FeS ₂	Fe, S, Cu	100
Ferrocolumbite	Carbonatites	4	0.5-1.0	(Fe,Mn,Mg)(Nb,Ta) ₂ O ₆	Fe, Nb, Ta, Mn, Si, Zr, Y ±Hf ±U	115-130
Ilmenite	Carbonatites	8	0.5-1.0	(Fe,Mg,Mn,Zn)(Ti,Nb)O ₃	Fe ±Ti, Nb ±Mn ±Si ±Zr	50-150
Magnetite	Carbonatites	2	0.5-1.0	AB ₂ O ₄ A = Fe, Mn, Mg, Zn, Co, Ni, Cu; B = Fe, Cr, Al, V, Mn, Ti	Fe, Si ±Ti ±Mn ±Cr	100-115
Nepheline	Ijolite	2	0.5-1.0	(Na,K,Ca)[Al(Si,Al)O ₄]	Si, Al, K, Ca, Rb, Sr	120
Olivine	Carbonatites	7	0.5-1.0	(Mg,Fe,Mn,Ca) ₂ [SiO ₄]	Fe, Si, Mn ±Mg	35-115
Orthoclase	Granite	1	20 x 40	(K,Na,Ba)[Al(Si,Al)Si ₂ O ₈]	Si, Al, K, Ba, Fe, Ca, Sr, Mn, Rb, Ti,	150
Pyroxene	Carbonatites, fenite	4	0.5-1.0	AB[(Si,Al) ₂ O ₆] A = Li, Na, Ca, Mg, Fe, Mn; B = Mg, Fe, Mn, Al, Cr, V, Sc, Ti	Si, Ca, Fe ±Mn ±K	100-120
Pyrochlore	Carbonatites	3	0.5-1.0	A _{2-x} B ₂ O ₆ (F,OH,O) _{1-y} A = Na, Ca, U, Sr, Y, REE, Th, Ba; B = Nb, Ta, Ti, Zr, Si, Fe	Nb, Ca, Ta, U, Fe, Sr, Zr, Y ±Si ±S ±Ce ±Th	115-130
Titanite	Fenite, ijolite	2	0.5-1.0	AB[SiO ₄](O,F) A = Ca, Na, Y, REE, Sr, Mn, Mg; B = Ti, Sn, V, Al, Ta, Nb, Zr, Fe	Ca, Ti, Fe, Zr, Nb, Sr, Y, ±Si ⁵	150
Zircon ⁵	Carbonatites	2	0.5-2.0	(Zr,Hf,U,Th,Y,REE)[SiO ₄]	Zr, Hf, Nb, Y	115-150
Zirconolite	Carbonatites	2	0.5-1.0	(Ca,Y,REE)Zr(Ti,Nb,Fe,Al) ₂ O ₇	Zr, Ti, Ca, Fe, Nb, Ta, Y, U, Hf, Sr ±Ce, ±Th	130-150

¹ Number of analyzed grains. ² Grain size in millimetres. ³ Total measurement time in seconds. ⁴ Rare earth elements. ⁵ Abundant Zr impedes Si detection due to spectral overlapping.

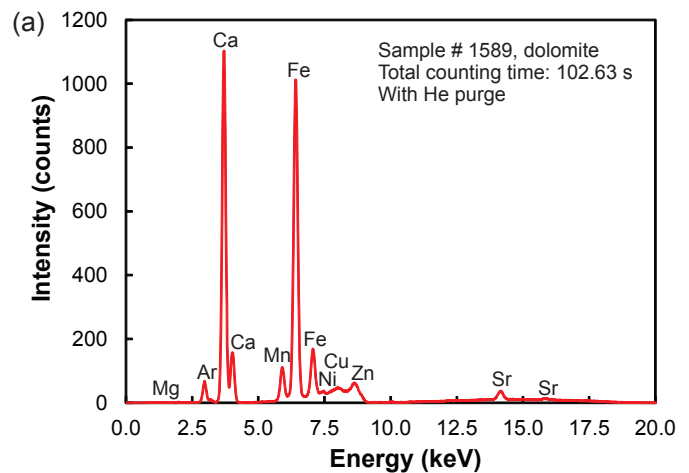
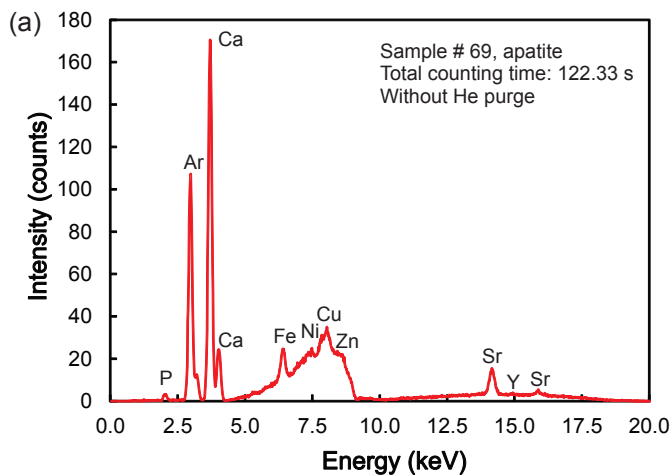
and Light energy filters were enabled to analyze samples containing these elements (Table 1). The measurements were 15-30 seconds each per energy range, except for the Light range elements, which were typically measured for 60 seconds. Although longer counting generally improves precision of the XRF analysis (e.g., Rukhlov, 2013), the total measurement time of 100-150 seconds provided acceptable counting statistics for detecting essential elements.

3. Results

We performed qualitative ED-XRF measurements on a total of 60 grains of different minerals (Table 1). An Ar peak was present in the X-ray spectra for all measurements (Figs. 3-9), except for a 2x4 cm orthoclase megacryst (larger than the instrument 8 mm sample spot; Fig. 7c). Although the pXRF detection system cannot resolve ArK α (2.958 keV) and AgL α (2.984 keV) energies, we attribute the Ar peak to the excitation

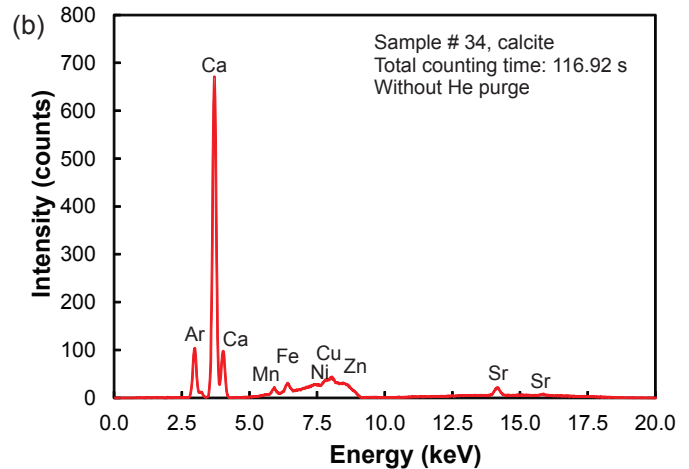
Table 2. Measurement conditions using Niton FXL “Mining” protocol in this study.

Filter ¹	Optional	Counting time (s)	Analyzed elements
Main	No	15-30	Mn, Fe, Co, Ni, Cu, Zn, As, Se, Rb, Sr, Y, Zr, Nb, Mo, Ag, Cd, Sn, Sb, Hf, Ta, W, Re, Au, Pb, Bi, Th, U
Low	Yes	15-30	K, Ca, Ti, V, Cr
High	Yes	0-30	Ag, Cd, Sn, Sb, Ba, La, Ce, Pr, Nd
Light	Yes	0-60	Mg, Al, Si, P, S, Cl

¹ X-ray energy range.

(b)

Elem	%	±2σ
Al	< LOD	0.926
Si	3.071	0.284
P	10.327	0.428
S	< LOD	0.187
Cl	1.119	0.070
K	< LOD	0.227
Ca	27.390	1.093
Ti	< LOD	0.616
Mn	< LOD	0.248
Fe	0.264	0.083
Sr	0.747	0.044
Y	0.014	0.003

**Fig. 4.** pXRF low energy filter X-ray spectra on single carbonate mineral grains (0.5-1.0 mm). **a)** Dolomite measured with He purge. **b)** Calcite measured with air in the X-ray path.**Fig. 3.** Representative pXRF measurement on a single apatite grain (0.5 mm). **a)** Low-energy filter X-ray spectrum. **b)** Instrument readout of the elemental abundances based on a factory-calibrated Mining protocol. Although the results are qualitative, relatively high Ca and P abundances, coupled with detectable Sr and Y, confirm apatite.

of air containing ~0.9% Ar in the X-ray path while measuring <1 mm-diameter samples on the instrument with 8 mm sample spot (K. Grattan, pers. comm. 2017). Due to using the Ag X-ray

tube, all X-ray spectra had an elevated background or ‘hump’ in the region corresponding to the characteristic X-ray energies of Ni, Cu, and Zn (Figs. 3-9), thus yielding false minor abundances of these elements in most measurements. In addition, minor Cl detected in most measurements (Table 3) is likely due to unresolved spectral interferences in the low-energy range of the X-ray spectrum. Therefore, we will not further consider the results for Cl, Ar, Cu, Ni, and Zn.

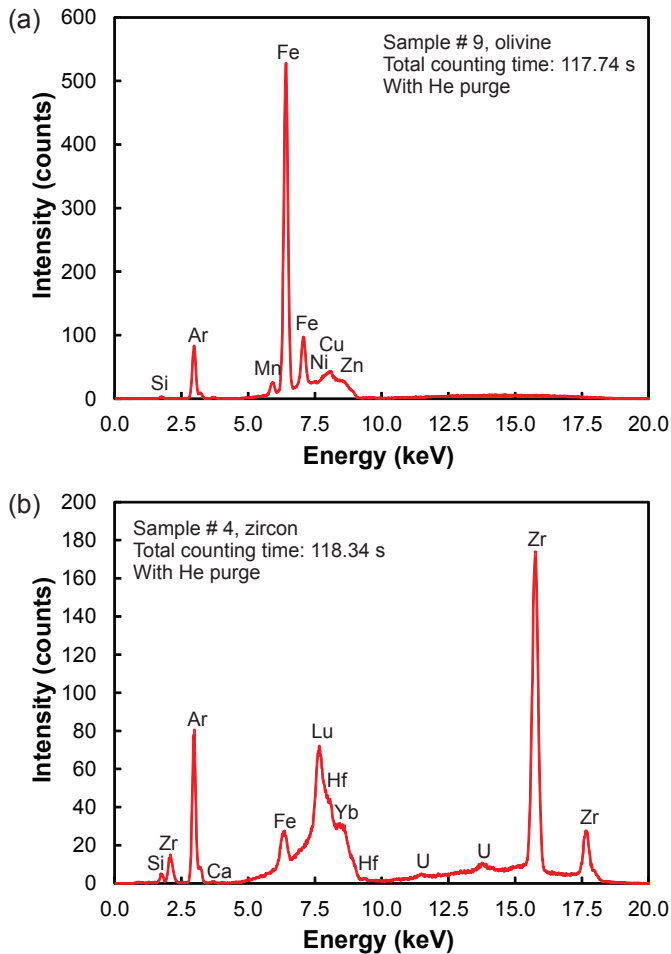


Fig. 5. pXRF low energy filter X-ray spectra on single silicate grains (0.5-2.0 mm) measured with He purge. a) Olivine. b) Zircon.

3.1. Apatite

We measured 13 apatite grains ranging from 0.5 to 1.0 mm. Two measurements were carried out with He in the X-ray path, which improved counting statistics only for Mg compared to those with air (Table 3). The pXRF measurements yielded essential Ca and P concentrations, as expected in apatite, along with relatively minor Si, Fe, Sr, and $Y \pm S \pm Ce \pm Th$ (Fig. 3), thus readily identifying the apatite grains.

3.2. Carbonate minerals

For two dolomite samples and one calcite sample (Table 1), the pXRF measurements yielded different proportions of the essential elements. Calcite yielded much higher Ca/(Fe, Mg, Mn) ratios than those of the dolomites, though Mg was detected only in measurements with He, which improved counting statistics on this element by an order of magnitude relative to the measurement with air in the X-ray path (Fig. 4; Table 3). The pXRF measurements also detected minor Sr and Si (Table 3).

3.3. Silicate minerals

3.3.1. Olivine

Six olivine samples from the Blue River carbonatites (Table 1) were measured with a He purge, whereas one sample was analyzed with air in the X-ray path. Main energy range elements were analyzed for 35 seconds. Counting statistics were similar to those for the longer measurements (100-115 seconds) using all four energy filters. All measurements showed essential Fe and Si abundances, coupled with relatively minor Mn and $Ca \pm S \pm Sr \pm Zr \pm Nb \pm Th$, with Mg detected only in one measurement made with He in the X-ray path (Fig. 5a; Table 3).

3.3.2. Zircon

Two pXRF measurements performed on zircon crystals from carbonatites (Table 1) yielded essential Zr abundances, coupled with relatively low Y, Nb, and Hf contents (Table 3; Fig. 5b). Other elements, including Si, were below the detection limits. Generally, the detection limits for low atomic number elements were much higher than those measured by pXRF on other minerals. Despite the poor counting statistics, the Si peak just visible in the X-ray spectrum, along with the prominent Zr peak at 15.78 keV (Fig. 5b), clearly identified zircon.

3.3.3. Titanite

Two titanite crystals from ijolite and fenite (Table 1) were measured for 150 seconds each using all four energy filters with air in the X-ray path. The pXRF measurements revealed essential Ti, Ca, and Si, along with minor Fe, Nb, Zr, Y, and Sr (Table 3), consistent with the available EPMA data on titanites from Blue River alkaline rocks (Mitchell et al., 2017). Similar to zircon, elevated Nb and Zr in titanite interfere with the low-energy range of the X-ray spectrum, resulting in elevated background for Si, Al and other elements (Table 3). However, the essential elements detected by pXRF (Fig. 6a) unambiguously identified titanites.

3.3.4. Pyroxenes and amphiboles

We measured four clinopyroxene (diopside to aegirine-augite) and one amphibole (actinolite-richterite) from carbonatites for 100-150 seconds (Table 1). Helium used in two measurements did not improve counting statistics relative to the analysis with air in the X-ray path. For diopside and amphibole, pXRF measurements detected essential Si, Ca, and Fe abundances, with diopsides showing much higher Si/Ca and Ca/Fe ratios than those of amphibole (Figs. 6b and d; Table 3). Minor $Mn \pm Sr \pm Zr \pm Nb \pm Th$ abundances indicate both substitutions (e.g., Mn) and inclusions (e.g., zircon and Nb-Ta oxides) in these minerals. Aegirine-augite yielded prominent Si and Fe abundances, along with detectable Mn, K and Rb. Calcium was not detected (Fig. 6c; Table 3), consistent with the mineral chemistry (Chudy, 2013; Mitchell et al., 2017). It should be noted that the Niton FXL instrument cannot detect elements with atomic number lower than Mg ($Z=12$), thereby limiting its application on Na-minerals. Although some modern

Table 3. Representative pXRF measurements on single grains of different minerals. All results are qualitative and provide only relative abundances of elements based on a factory-calibrated Mining protocol. LOD = Limit of detection based on the counting statistics (2σ error of the measurement); <LOD results are less than quoted 2σ values. NA = not analyzed; dash denotes missing values for elemental ratios owing to results <LOD or not determined.
[†] Analysis also yielded 3.2 ± 0.2 wt.% Cu.

Mineral	Apatite		Dolomite		Calcite		Olivine		Diopside	
	wt.%	2σ	wt.%	2σ	wt.%	2σ	wt.%	2σ	wt.%	2σ
Sample No.	1584	8	1580	1589	34	1579	9	10		
Counting (s)	102.97	117.15	102.97	102.63	116.92	101.45	117.74	118.65		
He purge	No	Yes	No	Yes	No	No	Yes	Yes		
Element	wt.%	2σ	wt.%	2σ	wt.%	2σ	wt.%	2σ	wt.%	2σ
Si	1.122	0.137	2.340	0.157	0.786	0.096	0.542	0.040	0.994	0.119
Ti	<LOD	0.248	<LOD	0.406	<LOD	0.116	<LOD	0.097	<LOD	0.223
Al	<LOD	0.418	<LOD	0.288	<LOD	0.235	<LOD	0.064	<LOD	0.405
Fe	<LOD	0.058	0.096	0.053	0.716	0.042	4.815	0.087	0.115	0.037
Mn	<LOD	0.127	<LOD	0.172	0.079	0.050	0.573	0.043	0.229	0.077
Mg	<LOD	2.861	<LOD	0.649	<LOD	1.646	1.461	0.195	<LOD	2.483
Ca	22.101	0.525	24.825	0.640	10.587	0.240	17.969	0.236	31.882	0.589
K	<LOD	0.104	<LOD	0.108	<LOD	0.066	<LOD	0.036	<LOD	0.081
P	10.161	0.273	13.162	0.319	<LOD	0.070	<LOD	0.024	<LOD	0.087
S	<LOD	0.082	0.325	0.067	<LOD	0.053	<LOD	0.021	<LOD	0.064
Cl	0.390	0.028	0.431	0.028	0.239	0.017	0.078	0.006	0.291	0.022
Rb	<LOD	0.002	<LOD	0.002	<LOD	0.002	<LOD	0.002	<LOD	0.002
Sr	0.075	0.004	0.168	0.007	0.024	0.001	0.206	0.004	0.292	0.009
Y	0.008	0.001	0.022	0.002	<LOD	0.002	<LOD	0.002	0.003	0.001
Zr	<LOD	0.002	<LOD	0.003	<LOD	0.002	<LOD	0.002	<LOD	0.003
Nb	<LOD	0.002	<LOD	0.002	<LOD	0.002	<LOD	0.002	<LOD	0.002
Ba	<LOD	0.023	<LOD	0.028	<LOD	0.014	<LOD	0.013	<LOD	0.023
Ce	<LOD	0.033	0.077	0.028	<LOD	0.019	<LOD	0.017	<LOD	0.031
Hf	NA	NA	0.060	0.018	NA	NA	NA	NA	NA	NA
Ta	NA	NA	0.293	0.033	NA	NA	NA	NA	NA	NA
Th	<LOD	0.005	<LOD	0.007	<LOD	0.003	<LOD	0.004	<LOD	0.006
U	<LOD	0.003	<LOD	0.003	<LOD	0.002	<LOD	0.002	<LOD	0.003
Cr	<LOD	0.086	<LOD	0.142	<LOD	0.039	<LOD	0.030	<LOD	0.072
Ca/Fe	-	259	14.8	3.73	277	-	-	-	277	11.6
Ca/Mn	-	-	134	31.4	139	-	-	-	139	-
Ca/Mg	-	-	-	12.3	-	-	-	-	-	-
Si/Ca	0.05	0.09	0.07	0.03	0.03	-	-	-	0.03	2.35

Table 3. Continued.

Mineral	Aegirine		Amphibole		Titanite		Zircon		Ilmenite		Magnetite		Fe sulphide ¹		
	wt.%	2σ	wt.%	2σ	wt.%	2σ	wt.%	2σ	wt.%	2σ	wt.%	2σ	wt.%	2σ	
Sample No.	1576	57	56	74	4	1586	1585	1578							
Counting (s)	101.92	152.10	150.04	153.29	118.34	104.05	101.09	101.39							
He purge	No	No	No	No	Yes	No	No	No							
Element	wt.%	2σ	wt.%	2σ	wt.%	2σ	wt.%	2σ	wt.%	2σ	wt.%	2σ	wt.%	2σ	
Si	4.568	0.190	13.710	0.426	6.755	0.370	17.97	<LOD	44.16	1.656	0.214	0.510	0.038	4.052	0.266
Ti	<LOD	0.138	<LOD	0.422	7.689	1.324	4.363	<LOD	0.085	6.617	1.336	<LOD	0.032	<LOD	0.193
Al	<LOD	0.250	<LOD	0.654	<LOD	0.495	1.762	<LOD	1.457	<LOD	0.507	<LOD	0.076	<LOD	0.734
Fe	1.965	0.061	12.930	0.407	0.235	0.072	0.185	<LOD	0.040	6.785	0.243	6.974	0.074	19.624	0.589
Mn	0.073	0.041	0.377	0.087	<LOD	0.256	0.313	<LOD	0.072	<LOD	0.370	0.041	0.022	<LOD	0.095
Mg	<LOD	1.635	<LOD	4.423	<LOD	3.686	15.32	<LOD	7.239	<LOD	3.867	<LOD	0.547	<LOD	5.301
Ca	<LOD	0.060	10.860	0.356	9.958	0.487	12.465	<LOD	0.019	<LOD	0.075	<LOD	0.010	<LOD	0.082
K	0.693	0.084	<LOD	0.132	<LOD	0.128	0.108	<LOD	0.047	<LOD	0.126	<LOD	0.021	<LOD	0.140
P	<LOD	0.074	<LOD	0.147	<LOD	0.144	89.160	<LOD	93.0	<LOD	0.155	<LOD	0.022	<LOD	0.146
S	<LOD	0.059	<LOD	0.112	<LOD	0.110	29.450	<LOD	50.21	<LOD	0.141	<LOD	0.017	8.086	0.271
Cl	0.261	0.020	0.606	0.039	0.605	0.044	0.198	<LOD	1.406	0.552	0.046	0.081	0.006	0.621	0.044
Rb	0.005	0.001	<LOD	0.002	<LOD	0.002	0.002	<LOD	0.002	<LOD	0.002	<LOD	0.002	<LOD	0.002
Sr	<LOD	0.002	0.003	0.001	0.003	0.001	0.059	0.027	<LOD	<LOD	0.002	<LOD	0.002	0.002	0.001
Y	<LOD	0.002	<LOD	0.002	0.010	0.001	0.026	0.012	0.023	0.014	0.002	<LOD	0.002	<LOD	0.002
Zr	<LOD	0.002	0.002	0.001	0.024	0.002	0.169	0.079	7.831	4.764	0.001	<LOD	0.002	<LOD	0.002
Nb	<LOD	0.002	<LOD	0.002	0.011	0.001	0.244	0.115	0.012	0.008	0.004	<LOD	0.002	<LOD	0.002
Ba	<LOD	0.013	<LOD	0.036	<LOD	0.025	0.026	<LOD	<LOD	0.023	<LOD	<LOD	0.008	<LOD	0.039
Ce	<LOD	0.017	<LOD	0.048	<LOD	0.034	0.048	<LOD	<LOD	0.031	<LOD	<LOD	0.011	<LOD	0.056
Hf	NA	NA	NA	NA	NA	NA	0.194	0.119	NA	NA	NA	NA	NA	NA	NA
Ta	NA	NA	NA	NA	NA	NA	<LOD	0.027	NA	NA	NA	NA	NA	NA	NA
Th	<LOD	0.003	<LOD	0.007	<LOD	0.005	<LOD	0.009	<LOD	0.013	0.007	0.003	0.001	<LOD	0.008
U	<LOD	0.002	<LOD	0.003	<LOD	0.002	<LOD	0.004	<LOD	0.009	0.003	<LOD	0.002	<LOD	0.003
Cr	<LOD	0.043	<LOD	0.137	<LOD	0.744	0.843	<LOD	<LOD	0.029	0.732	0.058	0.008	<LOD	0.073
Ca/Fe	-	-	0.84	-	42.4	-	34.2	-	-	-	-	-	-	-	-
Ca/Mn	-	-	28.8	-	-	-	-	-	-	-	-	-	-	-	-
Si/Ca	-	-	1.26	-	0.38	-	-	-	-	-	-	-	-	-	-
Fe/Ti	-	-	-	-	0.03	0.04	-	-	-	1.03	-	-	-	-	-

Table 3. Continued.

Mineral	Ferrocolumbite			Pyrochlore			Zirconolite			Albite			Orthoclase			Nepheline					
	48	46	47	1	45	66	59	51	71	wt.%	2 σ	No	wt.%	2 σ	No	wt.%	2 σ	No	wt.%	2 σ	No
Sample No.	131.63	133.7	134.92	117.37	133.00	153.41	107.49	151.94	120.11												
Counting (s)																					
He purge	No	No	No	Yes	No	No	No	No	No	No	No	No	No	No	No	No	No	No	No	No	No
Element	wt.%	2 σ	wt.%	2 σ	wt.%	2 σ	wt.%	2 σ	wt.%	2 σ	wt.%	2 σ	wt.%	2 σ	wt.%	2 σ	wt.%	2 σ	wt.%	2 σ	wt.%
Si	2.214	0.228	1.970	0.168	2.121	0.131	5.343	0.260	<LOD	27.39	<LOD	30.24	16.99	0.875	23.45	0.116	14.76	0.429			
Ti	<LOD	0.364	<LOD	0.346	<LOD	0.276	<LOD	0.631	4.243	2.500	3.677	2.078	<LOD	0.233	0.028	0.005	<LOD	0.183			
Al	<LOD	0.515	<LOD	0.371	<LOD	0.237	<LOD	0.295	<LOD	3.497	<LOD	2.958	<LOD	1.458	7.388	0.106	6.402	0.641			
Fe	3.437	0.100	3.233	0.086	0.086	0.018	1.281	0.083	1.439	0.835	1.113	0.582	<LOD	0.050	0.545	0.008	0.214	0.036			
Mn	0.253	0.068	0.296	0.058	<LOD	0.083	<LOD	0.173	<LOD	0.186	<LOD	0.255	<LOD	0.108	0.047	0.004	<LOD	0.091			
Mg	<LOD	3.491	<LOD	2.467	<LOD	1.489	<LOD	0.769	<LOD	28.77	<LOD	25.18	<LOD	6.631	<LOD	0.166	<LOD	2.733			
Ca	<LOD	0.066	<LOD	0.031	1.554	0.083	3.904	0.246	3.001	1.662	4.282	2.182	1.418	0.128	0.151	0.007	0.228	0.086			
K	<LOD	0.114	<LOD	0.083	<LOD	0.070	<LOD	0.138	<LOD	0.075	<LOD	0.089	<LOD	0.150	8.656	0.031	1.040	0.139			
P	<LOD	0.311	<LOD	0.235	<LOD	0.167	<LOD	0.22	<LOD	93.87	<LOD	93.63	<LOD	0.356	<LOD	0.011	<LOD	0.136			
S	<LOD	0.301	<LOD	0.231	<LOD	0.163	1.808	0.192	<LOD	56.94	<LOD	51.32	<LOD	0.295	0.021	0.006	<LOD	0.107			
Cl	0.558	0.044	0.381	0.030	0.303	0.021	0.545	0.039	<LOD	0.341	0.424	0.261	0.724	0.095	<LOD	0.003	0.458	0.036			
Rb	<LOD	0.002	<LOD	0.002	<LOD	0.004	<LOD	0.007	<LOD	0.002	<LOD	0.002	<LOD	0.002	0.033	0.001	0.005	0.001			
Sr	0.003	0.001	<LOD	0.002	0.070	0.003	0.179	0.011	0.005	0.003	0.018	0.010	0.073	0.003	0.091	0.001	0.042	0.002			
Y	0.002	0.001	0.003	0.001	0.006	0.001	0.005	0.003	0.064	0.037	0.168	0.092	<LOD	0.002	<LOD	0.002	<LOD	0.002			
Zr	0.045	0.003	0.035	0.003	0.022	0.002	0.013	0.006	4.584	2.652	3.487	1.926	<LOD	0.002	0.007	0.0003	<LOD	0.002			
Nb	5.815	0.201	5.584	0.177	4.409	0.113	8.963	0.564	0.827	0.479	0.199	0.111	0.002	0.001	<LOD	0.001	<LOD	0.002			
Ba	<LOD	0.033	<LOD	0.030	<LOD	0.020	<LOD	0.059	<LOD	0.023	<LOD	0.025	<LOD	0.020	0.615	0.005	NA	NA			
Ce	<LOD	0.046	<LOD	0.042	<LOD	0.028	<LOD	0.083	<LOD	0.078	0.213	0.128	<LOD	0.026	<LOD	0.007	NA	NA			
Hf	0.026	0.016	<LOD	0.032	<LOD	0.027	<LOD	0.050	0.080	0.048	0.097	0.053	NA	NA	<LOD	0.014	NA	NA			
Ta	1.075	0.046	2.650	0.074	3.710	0.078	5.100	0.233	0.349	0.204	0.172	0.093	NA	NA	<LOD	0.002	NA	NA			
Th	<LOD	0.027	<LOD	0.024	<LOD	0.021	<LOD	0.056	0.093	0.056	<LOD	0.015	<LOD	0.005	<LOD	0.003	<LOD	0.004			
U	<LOD	0.005	0.004	0.003	1.351	0.037	1.522	0.097	0.129	0.074	0.015	0.009	<LOD	0.002	0.002	0.001	<LOD	0.003			
Cr	<LOD	0.105	<LOD	0.099	<LOD	0.077	<LOD	0.181	<LOD	0.375	<LOD	0.389	<LOD	0.076	<LOD	0.105	<LOD	0.066			
Ca/Fe	-	-	18.1	-	1.37	-	3.05	-	2.09	-	3.85	-	-	0.28	-	-	1.07	-			
Si/Ca	-	-	1.37	-	1.37	-	1.37	-	-	-	-	-	12.0	156	-	-	64.7	-			
Al/K	-	-	-	-	-	-	-	-	-	-	-	-	-	-	0.85	-	6.16	-			
Si/K	-	-	-	-	-	-	-	-	-	-	-	-	-	-	2.71	-	14.2	-			
Fe/Nb	0.59	0.58	0.02	0.14	1.74	1.74	0.14	1.74	1.74	5.59	5.59	5.59	-	-	-	-	-	-			

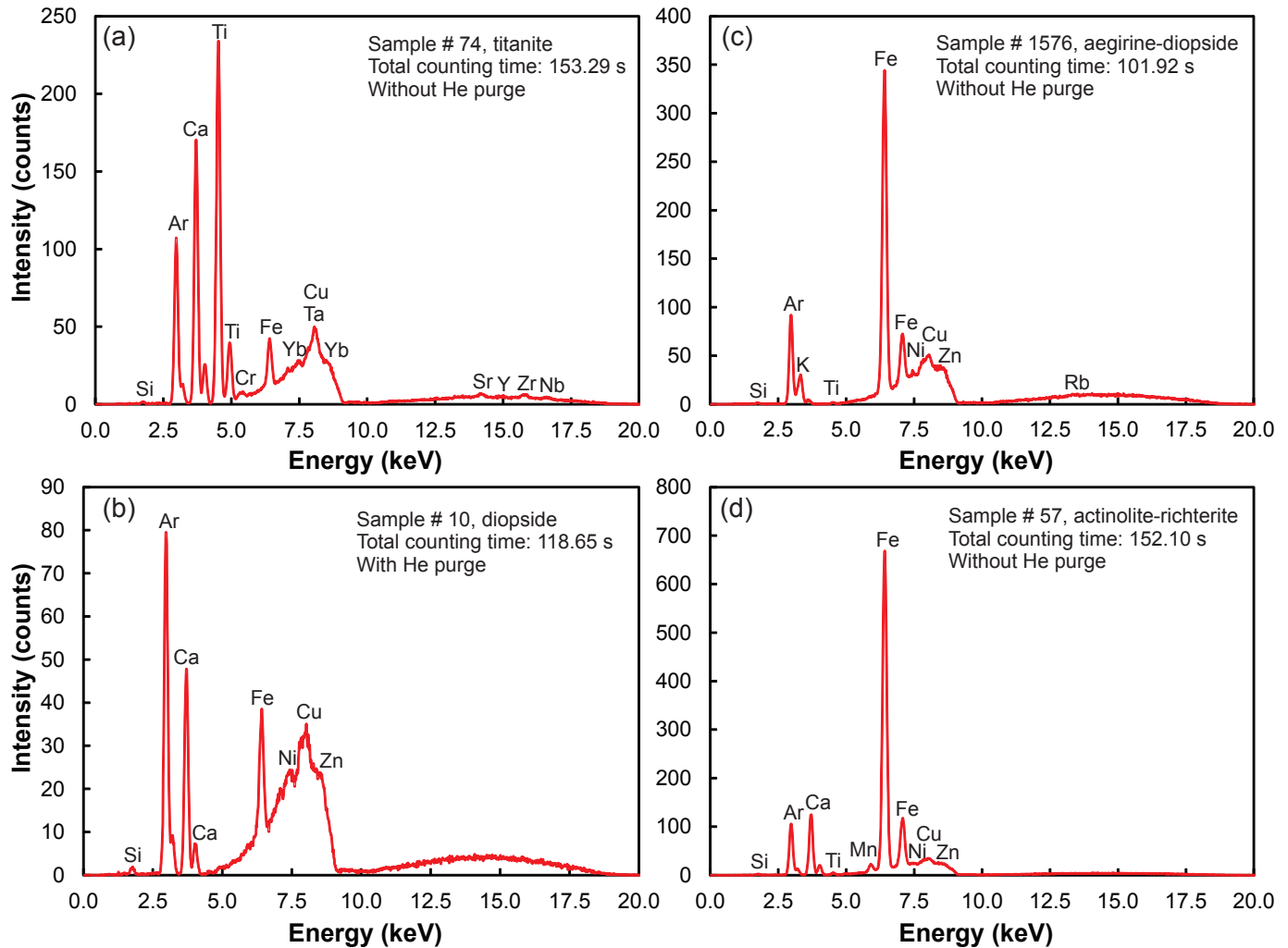


Fig. 6. pXRF low energy filter X-ray spectra on single silicate grains (0.5-1.0 mm). **a)** Titanite. **b)** Diopside. **c)** Aegirine-augite. **d)** Actinolite-richterite. All samples analyzed with air in the X-ray path, except (b) measured with He.

pXRF instruments capable of measuring Na and F (e.g., Bruker TRACER 5i) do not have this limitation, our results suggest that other elements in single-grain samples detected by pXRF readily identify pyroxenes and amphiboles.

3.3.5. Alkali feldspars and nepheline

We measured five albite ($\sim\text{An}_3$) and two nepheline single-grain (0.5-1.0 mm) samples from undersaturated alkaline rocks and fenites, and one orthoclase megacryst (2x4 cm; Table 1). All measurements, which were carried out for 105-150 seconds without He, yielded essential Si and minor Ca and $\text{Sr}\pm\text{Fe}\pm\text{Rb}\pm\text{Ba}$ abundances (Fig. 7; Table 3). Essential Al and K abundances were detected in orthoclase and nephelines but not in albites, with nephelines yielding much higher Al/K and Si/K ratios than those of orthoclase (Table 3). Although Na could not be measured using our pXRF instrument and hence alkali feldspars and feldspathoids cannot be unambiguously identified, our tests indicate that at least they can be distinguished from visually similar minerals (e.g., apatite) based on other essential elements (e.g., P).

3.4. Fe-Ti oxides

We performed pXRF measurements on two magnetite and eight ilmenite samples from carbonatites (Table 1). Total counting time was 50-150 seconds. Counting statistics for three ilmenites measured using He in the X-ray path did not improve compared to samples measured without He. The pXRF measurements readily distinguished between magnetites and ilmenites by different relative abundances of essential Fe and Ti in these minerals (Fig. 8). Minor elements detected by pXRF in the magnetites ($\text{Si}\pm\text{Mn}\pm\text{Cr}\pm\text{Nb}$) and ilmenites (Si , $\text{Nb}\pm\text{Mn}\pm\text{Ca}\pm\text{S}\pm\text{Sr}\pm\text{Zr}\pm\text{Ba}\pm\text{U}$) reflect common impurities in these minerals and possible inclusions (Table 3).

3.5. Rare-metal minerals

We analyzed single-grain samples of ferrocolumbite, pyrochlore, and zirconolite, which together with ilmenite, titanite, zircon and baddeleyite, are the principal hosts of Nb, Ta, Ti, Zr, Y, rare earth elements (REE), Th, and U in Blue River carbonatites and related rocks (Table 1).

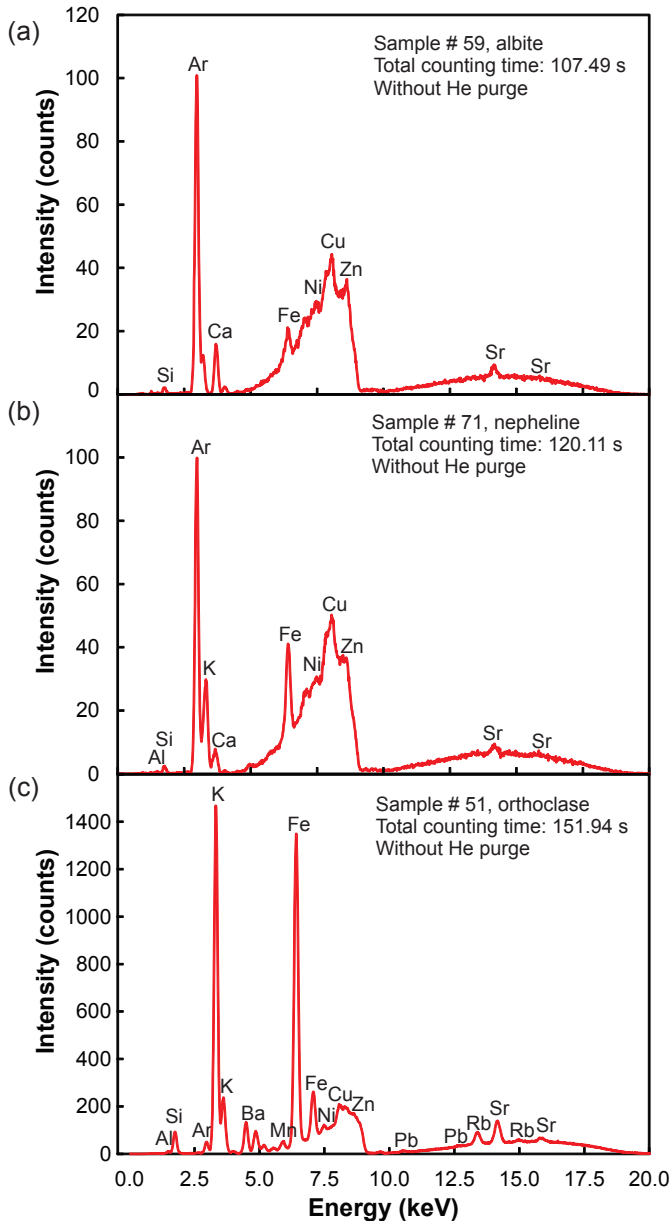


Fig. 7. pXRF low energy filter X-ray spectra on silicates measured with air in the X-ray path. **a)** Albite (~1 mm grain). **b)** Nepheline (~1 mm grain). **c)** Orthoclase megacryst (2x4 cm); note significant reduction of Ar peak compared with measurements on sand-size grains.

3.5.1. Ferrocolumbite

Four ferrocolumbite samples, measured 115-130 seconds each without He, yielded essential abundances of Fe and Nb, with minor Ta, Mn, Si, and Zr (Fig. 9a; Table 3). The qualitative pXRF results are generally consistent with ferrocolumbite compositions from Blue River carbonatites (Mariano, 1982; Chudy, 2013; Mackay and Simandl, 2015).

3.5.2. Pyrochlore

Measurements on three pyrochlore samples revealed essential Ca, Nb, Ta, and U abundances (Fig. 9b; Table 3), consistent with pyrochlore compositions from Blue River

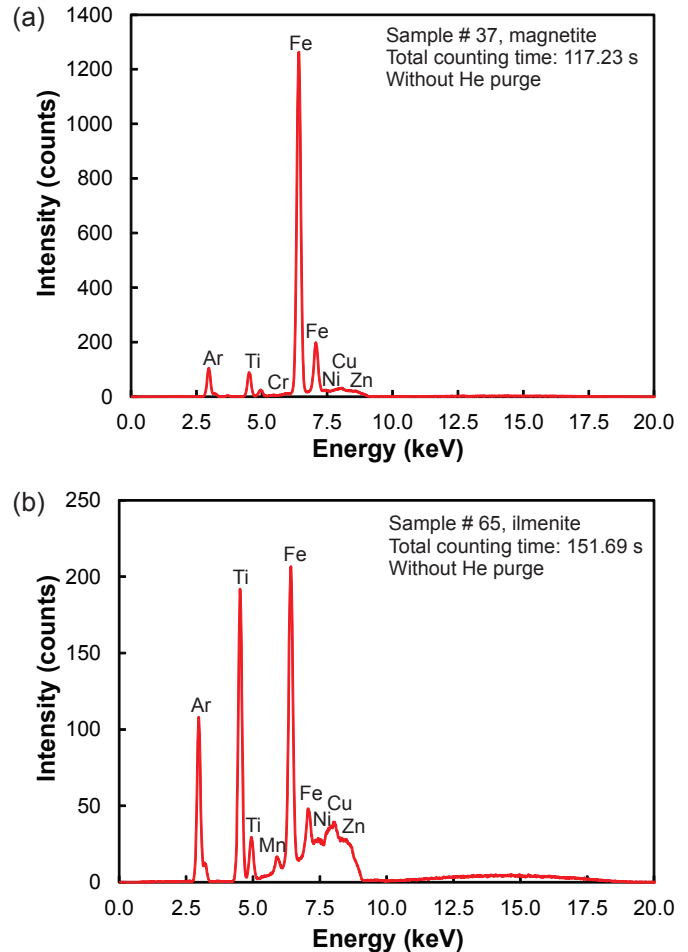


Fig. 8. pXRF low energy filter X-ray spectra on single Fe-Ti oxide grains (0.5-1.0 mm) measured with air in the X-ray path. **a)** Titanomagnetite. **b)** Ilmenite.

carbonatites (Mariano, 1982; Chudy, 2013; Mackay and Simandl, 2015). Minor elements detected by pXRF were Fe, Sr, Zr, Y±S±Ti±Ce±Th (Table 3). Although Si was also detected, we attribute it to Ta interference.

3.5.3. Zirconolite

pXRF measurements on two zirconolite samples (Table 1) readily detected essential Ti, Fe, Ca, Zr, and Nb, along with minor Sr, Y, Hf, Ta, and U±Ce±Th (Fig. 9c; Table 3). As with other Zr-rich minerals, spectral interference in the low-energy range of the X-ray spectrum rendered low-atomic number elements undetectable. Our qualitative pXRF results on single mineral grains are broadly consistent with the zirconolite chemistry (Mitchell et al., 2017) and thus demonstrate the effectiveness of pXRF for rapid identification of rare-metal minerals.

3.6. Other minerals

One pXRF measurement on a Fe sulphide grain (~0.5 mm) yielded essential Fe and S with less abundant Cu and Si

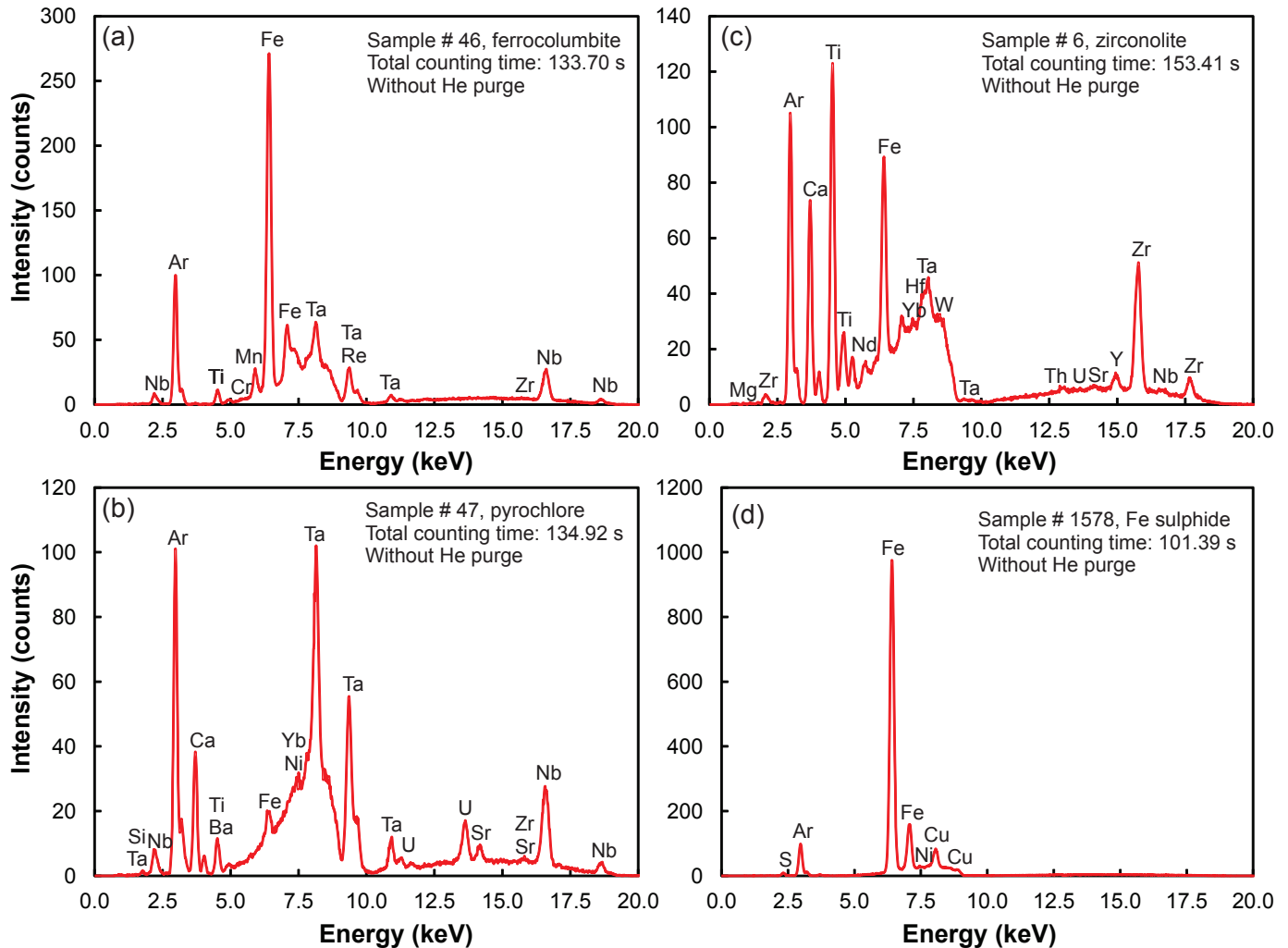


Fig. 9. pXRF low energy filter X-ray spectra on single grains of complex oxides and sulphide (0.5-1.0 mm) measured with air in the X-ray path. **a)** Ferrocolumbite. **b)** Pyrochlore. **c)** Zirconolite. **d)** Fe sulphide.

(Fig. 9c; Table 3), demonstrating the pXRF utility to confirm sulphides. Silicon likely reflects tiny amphiboles intergrown with the sulphide as suggested by petrographic examinations.

4. Discussion

Seventeen different minerals studied here, their general formulae, and essential and minor constituents detected by pXRF on single-grain (generally <1 mm) samples are summarized in Table 1. They include widespread rock-forming or accessory minerals that have a wide range of petrogenetic applications and are commonly recovered in indicator mineral surveys.

4.1. Significance of indicator minerals

Detrital dispersal of indicator minerals across a large area can be traced up the paleoflow direction to a much smaller source (Averill, 2001; McClenaghan, 2005; Gent et al., 2011; Lett and Rukhlov, 2018). Heavy (2.9-4.5 g·cm⁻³) and generally resistant to weathering, extensive solid-solution series within the

olivine, pyroxene and amphibole groups record crystallization conditions, and thus have a broad range of petrogenetic and mineral-exploration applications (e.g., Averill, 2001; Gent et al., 2011; Lett and Rukhlov, 2018). Although low-density (2.55-2.76 g·cm⁻³) feldspars and feldspathoids are usually not recovered in indicator mineral surveys, Williamson et al. (2016) suggested that plagioclase chemistry can be used as an exploration indicator for porphyry Cu deposits. Generally recessive for indicator mineral surveys, carbonates fix CO₂ and can concentrate Sr and REE, thereby making them important in stable and radiogenic isotopic applications among others (e.g., Rukhlov et al., 2015; Chakhmouradian et al., 2016).

Ubiquitous accessory or rock-forming minerals such as magnetite, ilmenite, titanite, zircon, and apatite have been widely used as indicator minerals and petrogenetic tools, because their chemistry fingerprints magmatic-hydrothermal processes and bedrock sources (Sha and Chappell, 1999; Hoskin and Ireland, 2000; Belousova et al., 2002a and b; Hayden et al., 2008; Bouzari et al., 2011, 2016; McLeod et al.,

2011; Gent et al., 2011; Carmody et al., 2014; Miles et al., 2014; Grimes et al., 2015; Bruand et al., 2016; Canil et al., 2016; Mao et al., 2016, 2017; Rukhlov et al., 2016, 2017; Smythe and Brennan, 2016). In addition, precise U-Pb ages and O-Hf-Nd isotopic compositions of detrital zircons provide insights into the Hadean crust-mantle evolution (e.g., Amelin et al., 1999; Wilde et al., 2001; Harrison et al., 2008).

Economic concentrations of minerals containing essential Nb±Ta±Ti±Zr±Hf±Y±U±Th±REE abundances are found mainly in carbonatites, related undersaturated rocks, and peralkaline complexes, with relatively minor production from granites, pegmatites and other sources (Mariano, 1989; Chakhmouradian, 2006; Chakhmouradian and Zaitsev, 2012; Mackay and Simandl, 2015; Mitchell, 2015). Burt (1989) listed about 190 minerals containing these elements as essential constituents. The most common minerals considered in this study are complex A-B oxides (A=Na, K, Ca, Fe²⁺, Mn, Mg, Sr, Ba, Pb, Y, REE, Th, and U; B=Al, Fe³⁺, V, Ti, Zr, Sn, Nb and Ta) such as pyrochlore (A_{2-x}B₂O₆(F,OH,O)_{1-y}·zH₂O), columbite (AB₂O₆), and zirconolite-zirkelite (AB₃O₇); zircon (ZrSiO₄); and titanite (ABSiO₃). Pyrochlore and ferrocolumbite are the major ore minerals in carbonatite-hosted Nb-Ta deposits in the Canadian Cordillera (Rowe, 1958; Mariano, 1982; Chudy, 2013; Chakhmouradian et al., 2015). Zirconolite was also found in Cordilleran carbonatites (A.N. Mariano, pers. comm., 1993, cited by Williams and Gieré, 1996) but analytical data were not available until recently. Millonig et al. (2012, 2013) reported accessory zirconolite (0.4-0.6 mm) associated with biotite, sulphides, magnetite, ilmenite, zircon, and baddeleyite in a carbonatite of the Blue River area. Mitchell et al. (2017) also noted rare zirconolite as inclusions in apatite and mantles (20-30 µm wide) on baddeleyite in some carbonatites and phoscoritic rocks at the Howard Creek locality mentioned by Williams and Gieré (1996). Because these minerals are resistant to physical and chemical weathering, they are useful indicators in exploration for Nb-Ta and REE deposits (Kogarko et al., 2013; Mackay and Simandl, 2015; Mackay et al., 2016).

4.2. Implications for mineral exploration

Regional geochemical surveys recovering heavy or indicator minerals from drainage and glacial deposits have been increasingly important for mineral exploration in regions covered by extensive overburden (e.g., Averill, 2001; McClenaghan, 2005; Gent et al., 2011; Lett and Rukhlov, 2018). Although bulk samples are usually processed for indicator minerals in the laboratory (McClenaghan et al., 2014; Plouffe et al., 2014), exploration companies and prospectors commonly examine the mineralogy of pan concentrates in the field (e.g., Gorham et al., 2009). However, visual identification and counting of worn detrital grains is challenging, because they lack crystal shape and may appear similar to other minerals. In our experience, 30-50% of grains hand-picked from 0.12-0.50 mm, 2.96-3.32 g·cm⁻³, non-paramagnetic (>1.2 A) fraction of granitic rocks were consistently rejected by EPMA as non-apatites (Mao et al., 2016). Though commercial laboratories

routinely check ambiguous mineral grains by SEM-EDS (e.g., Averill and Huneault, 2006), we applied the Niton FXL pXRF instrument in search of a rapid, in-field method of confirming ambiguous mineral grains.

Our qualitative pXRF measurements (30-150 seconds) on sand-size, single grains of different minerals demonstrate that essential constituents in minerals are readily detectable (Tables 1 and 3) using a factory-calibrated instrument, equipped with a standard 8 mm-wide sample spot, thereby providing a means to identify ambiguous grains. Although we used a benchtop pXRF instrument ideal for in-house applications, widely available hand-held pXRF instruments can be easily used in a benchtop mode with auxiliary test stands (Thermo Scientific, 2011). Instruments equipped with a smaller sample spot (e.g., 3 or 1 mm in diameter) and an XY control of the spot position (Thermo Scientific, 2011) would be optimal for measuring small samples such as single grains of sand.

4.3. Instrumental limitations

Unlike larger ED-XRF instruments and some newer pXRF analyzers, the Niton pXRF detection system does not determine Na (Z=11) and hence cannot unambiguously identify minerals containing essential Na concentrations. Despite this fundamental limitation, our pXRF measurements on single grains of such minerals (e.g., alkali feldspars, feldspathoids, clinopyroxenes and amphiboles) demonstrate that these minerals could be distinguished from visually similar minerals (e.g., apatite) on the basis of other essential elements detected by pXRF (Tables 1 and 3).

The 50 kV Ag X-ray target on the Niton FXL 950 pXRF instrument used in this study yields a broad peak in the low-energy range of the X-ray spectrum at ~8 keV, thus overlapping the region of the characteristic X-ray lines for Ni, Cu, Zn and other elements (e.g., Fig. 3a). Consequently, most pXRF measurements in this study had false minor abundances of these elements. Although factory-calibrated pXRF instruments are capable of precise and accurate determination of these elements on conventional samples such as soils and pulps (e.g., Knight et al., 2013; Rukhlov, 2013; Ryan et al., 2017; Steiner et al., 2017), these protocols may be inadequate for small-size samples such as <1 mm-diameter single mineral grains. However, our measurement on an Fe-sulphide grain indicated Cu content (Fig. 9d; Table 3). More measurements on small grains of minerals containing Ni, Cu, and Zn will help evaluate if they can be determined by pXRF.

4.4. Air interference with measuring small grains

All pXRF measurements on <1 mm-diameter samples in this study yielded an Ar peak in the X-ray spectra (Figs. 3-9) due to excitation of air (~0.9% Ar) in the X-ray path with an 8 mm-diameter sample spot (K. Grattan, pers. comm., 2017). Because the Ar peak size is inversely related to sample size, it may overlap adjacent low-energy lines of elements in the sample (e.g., Si, S, Cl, K, P, and Ca) with measurements on very small grains. However, Ar did not affect qualitative

detection of the essential elements for 0.5-1.0 mm-size single grains. Furthermore, our measurements to confirm ambiguous mineral grains in other studies (Rukhlov et al., 2017; Mao et al., 2018), on single grains as small as 0.12-0.25 mm, consistently detected P and Ca in apatite grains, suggesting that pXRF is a reliable, rapid method to confirm the identity of ambiguous grains.

4.5. Air versus helium in the X-ray path

Replacing air in the X-ray path with He is recommended for pXRF applications to low atomic number elements such as Mg, Al, Si, P, S and Cl (Thermo Scientific, 2011). Using He with the pXRF measurements in this study improved counting statistics (and hence detection limits) up to an order of magnitude only for Mg in some measurements on apatites, dolomites, and olivines (Table 3). However, He did not make a significant difference for detecting Mg in other minerals. Although Mg is an essential element in dolomites and olivines (Table 1), with the olivines from Blue River carbonatites containing 77-88 mol.% Mg_2SiO_4 end-member (Mariano, 1982; Mitchell et al., 2017), Mg was below the detection limit in these minerals measured with air in the X-ray path. These results illustrate the limitation of pXRF instruments for Mg determination on small samples. However, even with undetectable Mg, our pXRF measurements distinguished other essential elements in carbonate minerals (Ca-Fe-Mn) and olivine (Si-Fe-Mn). Helium did not significantly improve the detection limits for other low-atomic number elements, which were also generally detectable with air in the X-ray path in this study.

4.6. Spectral interferences

Magmatic carbonates and carbonatitic apatites are typically Sr-rich (Chakhmouradian et al., 2016, 2017; Mao et al., 2016). Although Si commonly substitutes into apatite via charge compensating reactions (see Mao et al., 2016 for an overview), minor Si detected by pXRF in apatites and carbonates in this study (Table 3) is likely due to Sr interference, because the pXRF detection system (~0.16 keV resolution) cannot resolve the $SiK\alpha$ (1.740 keV) and $SrL\alpha$ (1.807 keV) X-ray energies. Similarly, minor Si detected in Ta-rich pyrochlores is likely due to the Ta interference (Table 3).

Although Cl can be present in some mineral (e.g., apatites and amphiboles), minor Cl detected by pXRF for most samples in this study (Table 3) likely reflects unresolved spectral interferences in the low-energy range of the X-ray spectrum. Therefore, pXRF on small single grains cannot reliably determine Cl. Similarly, we attribute minor Hf and Ta detected in some apatites, olivines and diopsides (Table 3) to unresolved spectral interferences.

Detection limits for Mg, Al, Si, P, S and Cl in the pXRF measurements on Zr-rich minerals (zircon, titanite, zirconolite) were much higher than those on other minerals (Table 3). The poor counting statistics on these elements, due to the strong $Zr\pm Nb\pm Y$ interference on the low-energy range of the X-ray spectrum, thus somewhat limits pXRF application to identifying

Zr-bearing minerals. However, visual characteristics of these minerals, coupled with the robust detection of Ca, Ti, Fe, Y, Zr, Nb and other elements by pXRF (Figs. 5b, 6a and 9c), unambiguously identify these minerals.

4.7. Influence of inclusions in mineral grains

Relatively minor $Ca\pm Sr\pm Zr\pm Nb\pm Th$ detected by pXRF in some olivines, $Mn\pm Sr\pm Zr\pm Nb\pm Th$ in clinopyroxenes and amphibole, and Si in Fe-sulphide (Table 3) may reflect both inclusions of other minerals and chemical impurities (e.g., Ca in olivine and Mn in clinopyroxene and amphibole). However, traces of these elements could also be falsely detected by pXRF due to unresolved spectral interferences, especially in the low-energy range of X-ray spectrum as discussed above. As far as essential elemental abundances are concerned, the uncertain minor elements detected by pXRF will not impact the decision making with ambiguous mineral grains.

5. Future work

Our results demonstrate that qualitative pXRF is a powerful, rapid technique to identify sand-size, single mineral grains recovered in indicator mineral surveys. Although the pXRF measurements identified 17 different minerals in this study, future work is needed to test the technique on minerals containing essential Ni, Cu, Zn and other elements (e.g., As, Sb, REE). Systematic measurements on different minerals will help develop an algorithm that would improve the confidence of visual mineral identification using the qualitative pXRF element determinations. Low limits of detection for most elements determined by pXRF instruments permit first-order, in-field applications to distinguish indicator minerals based on mineral chemistry, such as for kimberlites (e.g., Cr-pyrope and Cr-diopside).

6. Conclusions

We tested pXRF instrument on single-grain (0.5-1.0 mm) samples of 17 different rock-forming and accessory minerals. Sixty qualitative measurements (30-150 seconds) using a factory-calibrated Mining mode based on fundamental parameters demonstrate that essential constituents detected by pXRF readily identify the minerals, thereby providing a new efficient, in-field technique for indicator mineral surveys and laboratory applications.

Acknowledgments

We thank Keith Grattan (Elemental Controls Limited) for discussion of the X-ray spectra and Ray Lett (British Columbia Geological Survey Emeritus Scientist), Ross Knight (Geological Survey of Canada) and Larry Aspler (British Columbia Geological Survey) for thorough reviews of the paper.

References cited

- Amelin, Y., Lee, D.C., Halliday, A.N., and Pidgeon, R.T., 1999. Nature of the Earth's earliest crust from hafnium isotopes in single detrital zircons. *Nature*, 399, 252-255.

- Averill, S.A., 2001. The application of heavy indicator mineralogy in mineral exploration with emphasis on base metal indicators in glaciated metamorphic and plutonic terrains. In: McClenaghan, M.B., Bobrowski, P.T., Hall, G.E.M., and Cook, S.J., (Eds.), *Drift Exploration in Glaciated Terrain*, Geological Society of London, Special Publication 185, pp. 49-82.
- Averill, S.A., and Huneault, R.G., 2006. Overburden Drilling Management Ltd: "Exploring Heavy Minerals". *Explore*, 133, 1-5.
- Belousova, E.A., Griffin, W.L., O'Reilly, S., and Fisher, N.I., 2002a. Apatite as an indicator mineral for mineral exploration: trace-element compositions and their relationship to host rock type. *Journal of Geochemical Exploration*, 76, 45-69.
- Belousova, E.A., Griffin, W.L., O'Reilly, S.Y., and Fisher, N.J., 2002b. Igneous zircon: trace element composition as an indicator of source rock type. *Contributions to Mineralogy and Petrology*, 143, 602-622.
- Bishop, J.L., Murad, E., Lane, M.D., and Mancinelli, R.L., 2004. Multiple techniques for mineral identification on Mars: A study of hydrothermal rocks as potential analogues for astrobiology sites on Mars. *Icarus*, 169, 311-323.
- Bouzari, F., Hart, C.J.R., Barker, S., and Bissig, T., 2011. Porphyry indicator minerals (PIMS): a new exploration tool for concealed deposits in south-central British Columbia. *Geoscience BC, Report 2011-17*, 31 p.
- Bouzari, F., Hart, C.J.R., Bissig, T., and Barker, S., 2016. Hydrothermal alteration revealed by apatite luminescence and chemistry: A potential indicator mineral for exploring covered porphyry copper deposits. *Economic Geology*, 111, 1397-1410.
- Bruand, E., Storey, C., and Fowler, M., 2016. An apatite for progress: Inclusions in zircon and titanite constrain petrogenesis and provenance. *Geology*, 44, 91-94.
- Bull, A., Brown, M.T., and Turner, A., 2017. Novel use of field-portable-XRF for the direct analysis of trace elements in marine macroalgae. *Environmental Pollution*, 220, 228-233.
- Burt, D.M., 1989. Compositional and phase relations among rare earth element minerals, Chapter 10. In: Lipin, B.R., and McKay, G.A., (Eds.), *Geochemistry and Mineralogy of Rare Earth Elements*, Mineralogical Society of America, *Reviews in Mineralogy*, 21, pp. 259-307.
- Canil, D., Grondahl, C., Lacourse, T., and Pisiak, L.K., 2016. Trace elements in magnetite from porphyry Cu-Mo-Au deposits in British Columbia, Canada. *Ore Geology Reviews*, 72, 1116-1128.
- Carmody, L., Taylor, L.A., Thaisen, K.G., Tychkov, N., Bodnar, R.J., Sobolev, N.V., Pokhilenko, L.N., and Pokhilenko, N.P., 2014. Ilmenite as a diamond indicator mineral in the Siberian craton: A tool to predict diamond potential. *Economic Geology*, 109, 775-783.
- Chakhmouradian, A.R., 2006. High-field-strength elements in carbonatitic rocks: geochemistry, crystal chemistry and significance for constraining the sources of carbonatites. *Chemical Geology*, 235, 138-160.
- Chakhmouradian, A.R., and Zaitsev, A.N., 2012. Rare earth mineralization in igneous rocks: sources and processes. *Elements*, 8, 347-353.
- Chakhmouradian, A.R., Reguir, E.P., Kressall, R.D., Crozier, J., Pisiak, L.K., Sidhu, R., and Yang, P., 2015. Carbonatite-hosted niobium deposit at Aley, northern British Columbia (Canada): Mineralogy, geochemistry and petrogenesis. *Ore Geology Reviews*, 64, 642-666.
- Chakhmouradian, A.R., Reguir, E.P., and Zaitsev, A.N., 2016. Calcite and dolomite in intrusive carbonatites. I. Textural variations. *Mineralogy and Petrology*, 110, 333-360.
- Chakhmouradian, A.R., Reguir, E.P., Zaitsev, A.N., Couëslan, C., Xu, C., Kynický, J., Mumin, A., and Yang, P., 2017. Apatite in carbonatitic rocks: Compositional variation, zoning, element partitioning and petrogenetic significance. *Lithos*, 274-275, 188-213.
- Chen, Z., Williams, N., and Zhang, H., 2013. Rapid and nondestructive measurement of labile Mn, Cu, Zn, Pb and As in DGT by using field portable-XRF. *Environmental Science: Processes & Impacts*, 15, 1768-1774.
- Chiari, G., Sarrazin, P., and Heginbotham, A., 2016. Non-conventional applications of a noninvasive portable X-ray diffraction/fluorescence instrument. *Applied Physics A: Materials Science and Processing*, 122, 1-17.
- Chudy, T.C., 2013. The petrogenesis of the Ta-bearing Fir carbonatite system, east-central British Columbia, Canada. Unpublished Ph.D. thesis, University of British Columbia, Canada, 316 p.
- Cohen, D.R., Cohen, E.J., Graham, I.T., Soares, G.G., Hand, S.J., and Archer, M., 2017. Geochemical exploration for vertebrate fossils using field portable XRF. *Journal of Geochemical Exploration*, 181, 1-9.
- Gent, M., Menendez, M., Toraño, J., and Torno, S., 2011. A review of indicator minerals and sample processing methods for geochemical exploration. *Journal of Geochemical Exploration*, 110, 47-60.
- Glanzman, R.K., and Closs, L.G., 2007. Field portable X-ray fluorescence geochemical analysis – Its contribution to onsite real-time project evaluation. In: Milkereit, B., (Ed.), *Proceedings of Exploration 07: Fifth Decennial International Conference on Mineral Exploration*, pp. 291-301.
- Gorham, J., Ulry, B., and Brown, J., 2009. Commerce Resources Corp. 2008 diamond drilling and exploration at the Blue River property, north of Blue River, British Columbia. British Columbia Ministry of Energy, Mines and Petroleum Resources, British Columbia Geological Survey, Assessment Report 31174, 149 p., 21 appendices.
- Grimes, C.B., Wooden, J.L., Cheadle, M.J., and John, B.E., 2015. "Fingerprinting" tectono-magmatic provenance using trace elements in igneous zircon. *Contributions to Mineralogy and Petrology*, 170, 1-26.
- Harrison, T.M., Schmitt, A.K., McCulloch, M.T., and Lovera, O.M., 2008. Early (≥ 4.5 Ga) formation of terrestrial crust: Lu-Hf, $\delta^{18}\text{O}$, and Ti thermometry results for Hadean zircons. *Earth and Planetary Science Letters*, 268, 476-486.
- Hayden, L.A., Watson, E.B., and Wark, D.A., 2008. A thermobarometer for sphene (titanite). *Contributions to Mineralogy and Petrology*, 155, 529-540.
- Hoskin, P.W.O., and Ireland, T.R., 2000. Rare earth element chemistry of zircon and its use as a provenance indicator. *Geology*, 28, 627-630.
- Knight, R.D., Kjarsgaard, B.A., Plourde, A.P., and Moroz, M., 2013. Portable XRF spectrometry of reference materials with respect to precision, accuracy, instrument drift, dwell time optimization, and calibration. *Geological Survey of Canada, Open File 7358*, 45 p.
- Kogarko, L.N., Sorokhtina, N.V., Kononkova, N.N., and Klimovich, I.V., 2013. Uranium and thorium in carbonatitic minerals from the Guli massif, Polar Siberia. *Geochemistry International*, 51, 767-776.
- Layton-Matthews, D., Hamilton, C., and McClenaghan, M.B., 2014. Mineral chemistry: modern techniques and applications to exploration. In: McClenaghan, M.B., Plouffe, A., and Layton-Matthews, D., (Eds.), *Application of Indicator Mineral Methods to Mineral Exploration*, 26th International Applied Geochemistry Symposium, Short Course SC07, November 17, 2013, Rotarua, New Zealand. Geological Survey of Canada, Open File 7553, pp. 9-18.
- Lett, R., and Rukhlov, A.S., 2017. A review of methods for regional geochemical surveys (RGS) in the Canadian Cordillera. In: Ferbey, T., Plouffe, A., and Hickin, A.S., (Eds.), *Indicator Minerals in Till and Stream Sediments of the Canadian Cordillera*. Geological Association of Canada Special Paper Volume 50, and Mineralogical Association of Canada Topics in Mineral Sciences Volume 47, pp. 53-108.
- Liritzis, I., and Zacharias, N., 2011. Portable XRF of archaeological

- artifacts: current research, potentials and limitations. In: Shackley, M.S., (Ed.), *X-Ray Fluorescence Spectrometry (XRF) in Geoarchaeology*, Springer, New York, pp. 109-142.
- Mackay, D.A.R., and Simandl, G.J., 2015. Pyrochlore and columbite-tantalite as indicator minerals for specialty metal deposits. *Geochemistry: Exploration, Environment, Analysis*, 15, 167-178
- Mackay, D.A.R., Simandl, G.J., Ma, W., Redfearn, M., and Gravel, J., 2016. Indicator mineral-based exploration for carbonatites and related specialty metal deposits – a QEMSCAN® orientation survey, British Columbia, Canada. *Journal of Geochemical Exploration*, 165, 159-173.
- Mao, M., Rukhlov, A.S., Rowins, S.M., Spence, J., and Coogan, L.A., 2016. Apatite trace element compositions: A robust new tool for mineral exploration. *Economic Geology*, 111, 1187-1222.
- Mao, M., Rukhlov, A.S., Rowins, S.M., Hickin, A.S., Ferbey, T., Bustard, A., Spence, J., and Coogan, L.A., 2017. A novel approach using detrital apatite and till geochemistry to identify covered mineralization in the TREK area of the Nechako Plateau, British Columbia. In: Ferbey, T., Plouffe, A., and Hickin, A.S., (Eds.), *Indicator Minerals in Till and Stream Sediments of the Canadian Cordillera*, Geological Association of Canada Special Paper Volume 50, and Mineralogical Association of Canada Topics in Mineral Sciences Volume 47, pp. 191-243.
- Mariano, A.N., 1982. Petrology, mineralogy and geochemistry of the Blue River carbonatites. Confidential report for Anshultz (Canada) Mining Ltd., 130 p.
- Mariano, A.N., 1989. Economic geology of rare earth minerals, Chapter 11. In: Lipin, B.R., and McKay, G.A., (Eds.), *Geochemistry and Mineralogy of Rare Earth Elements*, Mineralogical Society of America, *Reviews in Mineralogy*, 21, pp. 309-337.
- Martín-Peinado, F.J., and Rodríguez-Tovar, F.J., 2016. Researching protected geosites: in situ and non-destructive analysis of mass-extinction bioevents. *Geoheritage*, 8, 351-357.
- McClenaghan, M.B., 2005. Indicator mineral methods in mineral exploration. *Geochemistry: Exploration, Environment, Analysis*, 5, 233-245.
- McClenaghan, M.B., Plouffe, A., McMartin, I. J., Campbell, J.E., Spirito, W.A., Paulen, R.C., Garrett, R.G., and Hall, G.E.M., 2014. Till sampling and geochemical analytical protocols used by the Geological Survey of Canada. *Geochemistry: Exploration, Environment, Analysis* 2013, 13, 285-301.
- McLeod, G.W., Dempster, T.J., and Faithfull, J.W., 2011. Deciphering magma-mixing processes using zoned titanite from the Ross of Mull Granite, Scotland. *Journal of Petrology*, 52, 55-82.
- Miles, A.J., Graham, C.M., Hawkesworth, C.J., Gillespie, M.R., Hinton, R.W., Bromiley, G.D., and EMMAC, 2014. Apatite: a new redox proxy for silicic magmas? *Geochimica et Cosmochimica Acta*, 132, 101-119.
- Millonig, L.J., Gerdes, A., and Groat, L.A., 2012. U-Th-Pb geochronology of meta-carbonatites and meta-alkaline rocks in the southern Canadian Cordillera: a geodynamic perspective. *Lithos*, 152, 202-217.
- Millonig, L.J., Gerdes, A., and Groat, L.A., 2013. The effect of amphibolite facies metamorphism on the U-Th-Pb geochronology of accessory minerals from meta-carbonatites and associated meta-alkaline rocks. *Chemical Geology*, 353, 199-209.
- Mitchell, R.H., 2015. Primary and secondary niobium mineral deposits associated with carbonatites. *Ore Geology Reviews*, 64, 626-641.
- Mitchell, R., Chudy, T., McFarlane, C.R.M., and Wu, F.-Y., 2017. Trace element and isotopic composition of apatite in carbonatites from the Blue River area (British Columbia, Canada) and mineralogy of associated silicate rocks. *Lithos*, 286-287, 75-91.
- Palmer, T., Jacobs, R., Baker, E., Ferguson, K., and Webber, S., 2009. Use of field-portable XRF analyzers for rapid screening of toxic elements in FDA-regulated products. *Journal of Agricultural and Food Chemistry*, 57, 2605-2613.
- Pell, J., 1994. Carbonatites, nepheline syenites, kimberlites and related rocks in B.C. British Columbia Ministry of Energy, Mines and Petroleum Resources, British Columbia Geological Survey, Bulletin 88, 136 p.
- Piorek, S., 1994. Principles and applications of man-portable X-ray fluorescence spectrometry. *Trends in Analytical Chemistry* 13, 281-286.
- Plouffe, A., McClenaghan, M.B., Paulen, R.C., McMartin, I., Campbell, J.E., and Spirito, W.A., 2014. Processing of glacial sediments for the recovery of indicator minerals: protocols used at the Geological Survey of Canada. *Geochemistry: Exploration, Environment, Analysis*, 13, 303-316.
- Potts, P.J., and West, M., (Eds.), 2008. *Portable X-ray Fluorescence Spectrometry: Capabilities for In Situ Analysis*. Royal Society of Chemistry, 291 p.
- Quye-Sawyer, J., Vandeginste, V., and Johnston, K.J., 2015. Application of handheld energy-dispersive X-ray fluorescence spectrometry to carbonate studies: opportunities and challenges. *Journal of Analytical Atomic Spectrometry*, 30, 1417-1680.
- Rouillon, M., and Taylor, M., 2016. Can field portable X-ray fluorescence (pXRF) produce high quality data for application in environmental contamination research? *Environmental Pollution*, 214, 225-264.
- Rowe, R.P., 1958. Niobium (Columbium) deposits of Canada. Geological Survey of Canada, *Economic Geology Series*, 18, 108 p.
- Rukhlov, A.S., 2013. Determination of major and trace element concentrations in Canadian sediment reference samples using portable energy-dispersive X-ray fluorescence (ED-XRF) spectrometer and implications for geochemical surveys. British Columbia Ministry of Energy, Mines and Natural Gas, British Columbia Geological Survey GeoFile 2013-6.
- Rukhlov, A.S., Bell, K., and Amelin, Y., 2015. Carbonatites, isotopes and evolution of the subcontinental mantle: An overview. In: Simandl, G.J. and Neetz, M., (Eds.), *Symposium on Strategic and Critical Materials Proceedings*, November 13-14, 2015, Victoria, British Columbia, British Columbia Ministry of Energy and Mines, British Columbia Geological Survey, Paper 2015-3, pp. 39-64.
- Rukhlov, A.S., Plouffe, A., Ferbey, T., Mao, M., and Spence, J., 2016. Application of trace-element compositions of detrital apatite to explore for porphyry deposits in central British Columbia. In: *Geological Fieldwork 2015*, British Columbia Ministry of Energy and Mines, British Columbia Geological Survey, Paper 2016-1, pp. 145-179.
- Rukhlov, A.S., Rowins, S.M., Mao, M., Coogan, L.A., and Spence, J., 2017. Apatite compositions as a proxy for the oxidation states of porphyry Cu-Mo-Au deposits. British Columbia Ministry of Energy and Mines, British Columbia Geological Survey GeoFile 2017-2.
- Ryan, J.G., Shervais, J.W., Li, Y., Reagan, M.K., Li, H.Y., Heaton, D., Godard, M., Kirchenbauer, M., Whattam, S.A., Pearce, J.A., Chapman, T., Nelson, W., Prytulak, J., Shimizu, K., Petronotis, K., the IODP Expedition 352 Scientific Team, 2017. Application of a handheld X-ray fluorescence spectrometer for real-time, high-density quantitative analysis of drilled igneous rocks and sediments during IODP Expedition 352. *Chemical Geology*, 451, 55-66.
- Sarala, P., Taivalkoski, A., and Valkama, J., 2015. Portable XRF: an advanced on-site analysis method in till geochemical exploration. In: Sarala, P., (Ed.), *Novel Technologies for Greenfield Exploration*, Geological Survey of Finland, Special Paper 57, pp. 63-86.
- Sha, L.-K., and Chappell, B.W., 1999. Apatite chemical composition, determined by electron microprobe and laser-ablation inductively coupled plasma mass spectrometry, as a probe into granite

- petrogenesis. *Geochimica et Cosmochimica Acta*, 63, 3861-3881.
- Simandl, G.J., Paradis, S., Stone, R.S., Fajber, R., Kressall, R., Grattan, K., Crozier, J., and Simandl, L.J., 2014. Applicability of handheld X-ray fluorescence spectrometry in the exploration and development of carbonatite-related niobium deposits: a case study of the Aley Carbonatite, British Columbia, Canada. *Geochemistry: Exploration, Environment, Analysis*, 17, 211-221.
- Smythe, D.J., and Brenan, J.M., 2016. Magmatic oxygen fugacity estimated using zircon-melt partitioning of cerium. *Earth and Planetary Science Letters*, 453, 260-266.
- Steiner, A.E., Conrey, R.M., and Wolff, J.A., 2017. PXRF calibrations for volcanic rocks and the application of in-field analysis to the geosciences. *Chemical Geology*, 453, 35-54.
- Thermo Scientific, 2011. Thermo Fisher Scientific Niton Analyzers: FXL Users Guide, Version 8.0, Revision A, March 2011, 106 p.
- Weindorf, D.C., Castañeda, J.H.C., Bakr, N., and Swanhart, S., 2013. Direct soil gypsum quantification via portable X-Ray fluorescence spectrometry. *Soil Science Society of America Journal*, 77, 2071-2077.
- Wiedenbeck, M., 2013. Field-portable XRF: A geochemist's dream? *Elements*, 9, 7-8.
- Wilde, S.A., Valley, J.W., Peck, W.H., and Graham, C.M., 2001. Evidence from detrital zircons for the existence of continental crust and oceans on the Earth 4.4 Gyr ago. *Nature*, 409, 175-178.
- Williams, C.T., and Gieré, R., 1996. Zirconolite: a review of localities worldwide, and a compilation of its chemical composition. *Bulletin of the Natural History Museum: Geology Series*, 52, 1-24.
- Williamson, B.J., Herrington, R.J., and Morris, A., 2016. Porphyry copper enrichment linked to excess aluminium in plagioclase. *Nature Geoscience*, 9, 237-241.
- Young, K.E., Evans, C.A., Hodges, K., Bleacher, J.E., and Graff, T.G., 2016. A review of the handheld X-ray fluorescence spectrometer as a tool for field geologic investigations on Earth and in planetary surface exploration. *Applied Geochemistry*, 72, 77-87.
- Zhang, W., Lentz, D.R., and Charnley, B.E., 2017. Petrogeochemical assessment of rock units and identification of alteration/mineralization indicators using portable X-ray fluorescence measurements: Applications to the Fire Tower Zone (W-Mo-Bi) and the North Zone (Sn-Zn-In), Mount Pleasant deposit, New Brunswick, Canada. *Journal of Geochemical Exploration*, 177, 61-72.